ORIGINAL RESEARCH

Multifunctional Nanotheranostic Gold Nanocage/ Selenium Core-Shell for PAI-Guided Chemo-Photothermal Synergistic Therapy in vivo

Xueyang Fang
Kwok-Ho Lui
Shiying Li
Wai-Sum Lo
Xin Li
Yanjuan Gu
Wing-tak Wong

Department of Applied Biology and Chemical Technology, The Hong Kong Polytechnic University, Hong Kong Special Administrative Region, People's Republic of China

Introduction: Cancer theragnosis involving cancer diagnosis and targeted therapy simultaneously in one integrated system would be a promising solution of cancer treatment. Herein, a convenient and practical cancer theragnosis agent was constructed by combining gold nanocages (AuNCs) covered with selenium and a chitosan (CS) shell (AuNCs/Se) to incorporate the anti-cancer drug doxorubicin (DOX) as a multifunctional targeting nanocomposite (AuNCs/DOX@Se-iRGD) for photoacoustic imaging (PAI)-guided chemo-photothermal synergistic therapy that contributes to enhanced anti-cancer efficacy. The novel design of AuNCs/DOX@Se-iRGD gives the nanocomposite two outstanding properties: (1) AuNCs, with excellent LSPR property in the NIR region, act as a contrast agent for enhanced PAI and photothermal therapy (PTT); (2) Se acts as an anti-cancer nanoagent and drug delivery cargo.

Methods: The photothermal performance of these nanocomposites was evaluated in different concentrations with laser powder densities. These nanocomposites were also incubated in pH 5.3, 6.5, 7.4 PBS and NIR laser to study their drug release ability. The cellular uptake was studied by measuring the Se and Au concentrations inside the cells using inductively coupled plasma-mass spectrometry (ICP-MS). Besides, in vitro and in vivo anti-tumor activity were carried out by cytotoxicity assay MTT and tumor model nude mice, respectively. As for imaging, the PA value and images of these nanocomposites accumulated in the tumor site were sequentially collected at specific time points for 48 h.

Results and Discussion: The prepared AuNCs/DOX@Se-iRGD showed excellent biocompatibility and physiological stability in different media. In vivo results indicated that the targeting nanocomposite presented the strongest contrast-enhanced PAI signals, which could provide contour and location information of tumor, 24 h after intravenous injection. Likewise, the combined treatment of chemo- and photothermal synergistic therapy significantly inhibited tumor growth when compared with the two treatments carried out separately and showed negligible acute toxicity to the major organs.

Conclusion: This study demonstrates that AuNCs/DOX@Se-iRGD has great prospect to become a multifunctional anti-tumor nanosystem for PAI-guided chemo- and photothermal synergistic therapy.

Keywords: gold nanocage, nanocomposites, NIR, PA imaging, synergistic therapy

Correspondence: Yanjuan Gu; Wing-tak Wong
Department of Applied Biology and Chemical Technology, The Hong Kong Polytechnic University, Hung Hom, Kowloon, Hong Kong, People's Republic of China
Tel +852 3400 8858; +852 3400 8789
Fax +852 2364 9932
Email yanjuan.gu@polyu.edu.hk; w.t.wong@polyu.edu.hk

Introduction

Breast cancer is the most common disease and the primary cause of cancer death among women in the world.[1,2] Conventional therapies such as surgery, radiotherapy, and chemotherapy have their limitations such as adverse side effects, low bioavailability, and poor therapeutic efficiency.[3,4] To address the issue, combination

therapy that integrates various modalities such as chemotherapy, radiotherapy, photothermal therapy (PTT) and others into one platform has come under the spotlight due to its potential to increase drug accumulation in the target lesion and enhance cancer treatment efficacy.[5,6]

The chemotherapy-free drugs face a series of barriers such as poor solubility, lack of selectivity, severe side effects and poor delivery efficiency that limit their therapeutic effect.[7,8] To overcome these shortcomings, a wide variety of stimuli-responsive drug delivery nanosystems that control drug release precisely in particular tumor tissues, and thus improve drug accumulation and reduce side effects, have been invented. To date, nanosystems that respond to different stimulations, such as enzymes,[9] pH,[10–12] redox,[11] magnetic fields[11,13] and hyperthermia,[11,14] have been reported. Among these stimuli, near-infrared (NIR) laser-induced hyperthermia is a better choice because of its non-invasive nature and excellent tissue penetration capability. In this regard, plasmonic nanomaterials such as gold nanorods (AuNRs) and AuNCs, which are capable of controlling drug release due to their intense surface plasmon resonance (SPR) and low fluorescence quantum yield, have been regarded as potential candidates in PTT. Although the synergistic effect of combining PTT and chemotherapy has been presented by some nanocomposites based on their core-shell structure, such as polymer/nanoshell, mesoporous silica/gold nanoshell and gold nanorod-capped magnetic core/mesoporous silica,[15–17] there is still a need to fabricate targeting nanocomposites with high anti-cancer loading capacity for more effective cancer treatment.

Compared with Au nanoparticles, gold nanocages (AuNCs) have hollow interiors for higher anti-cancer drug loading capacity, higher photothermal conversion efficiency, tunable localized surface plasmon resonance (LSPR) band in the NIR region and excellent biocompatibility, making them ideal vehicles for controlled drug release. However, the intrinsic hollow interiors and pores of AuNCs could result in premature drug leakage in vivo, which restricts their therapeutic anticancer effect. Some groups have modified AuNCs with thermally responsive polymers, silica and cancer cell membrane to reduce premature release in blood circulation while the loaded drug could be released precisely at specific tumor tissue through a controllable stimulus, such as NIR laser irradiation[18–20] and pH.[21,22]

Numerous studies have suggested that co-delivery with selenium (Se) could reduce the side effects of chemotherapeutic drugs and decrease cancer incidence.[23] Selenium nanoparticles (SeNPs) have been studied and proposed as excellent nanomedicines for anti-tumor drugs and drug carrier because of their high anti-tumor activity, superior anti-oxidation, low toxicity to normal cells, and good biocompatibility and degradability. Chen's group[24–27] reported that SeNPs induced apoptosis in tumor cells by causing intracellular oxidative stress, mitochondrial dysfunction and simultaneous inhibition of cancer growth, migration and invasion. Kim's group[28] reported that silica-capped gold nanorods covered with Se coating (Se@Au@mSiO$_2$/DOX) suppressed tumor cell growth by cell cycle arrest and induced apoptosis via suppression of the Src/FKA/AKT signaling pathways. This indicated that nanocomposites containing Se showed significant tumor growth suppression capability.

Recently, PAI has emerged as a novel non-invasive imaging modality achieving submillimeter resolution at depths of 7–10 cm in vivo. It combines the high spatial resolution of ultrasound and the high contrast of optical imaging to provide fast, quantitative and volumetric measurement with deep tissue penetration capability.[29,30] Although PAI was initially employed for imaging endogenous chromophores such as hemoglobin, more and more exogenous imaging agents with tumor-targeting nanoplatforms have gained attention as they are able to further increase the contrast of the targeting tumor sites or visualize target-specific molecular processes.[31–34] Herein, we report a novel PAI-guided, hyperthermia-triggered nanocomposite (AuNCs/DOX@Se-iRGD) for controlled drug release to inhibit tumor growth. As illustrated in Scheme 1, the nanocomposite had an AuNCs core that worked as a PAI contrast agent and photothermal agent, and Se/CS shells that act as a supporter to enhance anti-cancer drug loading capacity and as a NIR stimuli gatekeeper. The AuNCs absorb and convert NIR light into heat for controlling DOX release from both the inner AuNCs and Se/CS shells. The surface decoration of iRGD on the nanocomposite significantly enhanced cellular uptake in cancer cells. The combined therapeutic effect of Se, PTT and chemotherapy of the nanocomposite on tumor growth inhibition was evaluated by using MCF-7 breast cancer model in vivo.

Materials and Methods
Materials
Gold (III) chloride trihydrate, sodium citrate tribasic dehydrate, sodium borohydride, hydroxylamine, sodium selenite
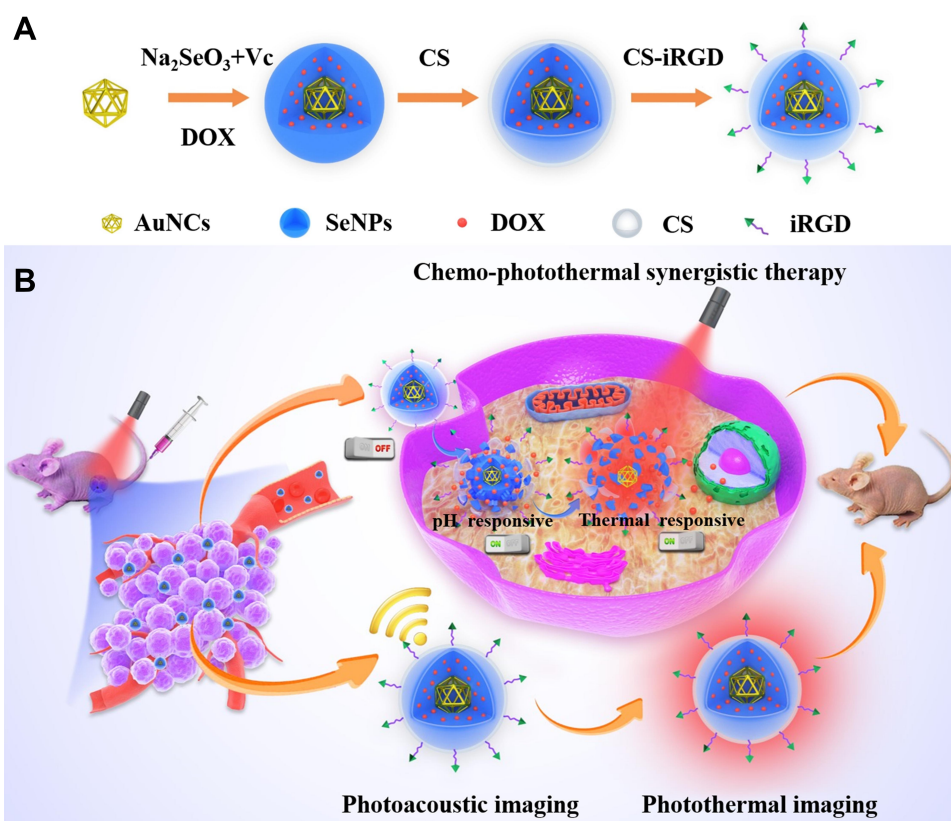
Scheme 1 (**A**) Schematic illustration of design and preparation process of AuNCs/DOX@Se-iRGD; (**B**) Schematic illustration of AuNCs/DOX@Se-iRGD as a multifunctional nanocomposite for chemo-photothermal synergistic therapy and imaging.

(Na_2SeO_3), L-ascorbic acid (Vitamin C, Vc), chitosan (CS, MW: 50~190 KDa), doxorubicin HCl (DOX), N-hydroxysuccinimide (NHS), 1-(3-Dimethylaminopropyl)-3-ethylcarbodiimide hydrochloride (EDC), thiazolyl blue tetrazolium bromide (MTT), propidium iodide (PI), calcein-AM, sliver nitrate were purchased from Sigma-Aldrich. Mercapto polyethylene glycol carboxyl group (SH-PEG-COOH, MW: 2000) was purchased from Shanghai Tuoyang Biotechnology Co., LTD. iRGD was purchased from GL Biochem (Shanghai) Ltd. The dialysis membrane (MWCO: 12~14 KDa) was purchased from Spectrum Laboratories, Inc. All cell culture media were purchased from Thermo Fisher (Hong Kong, China). Milli-Q water was applied in all experiments.

Preparation of CS-iRGD

CS-iRGD was prepared through the formation of an amide bond between CS and iRGD as previously described.[35] iRGD (5mg) was dissolved in deionized water, and then NHS and EDC were added as an amidation catalyst to activate iRGD. After stirring the solution for 2 h at room temperature, CS solution was added and the mixed solution was stirred for an additional 8 h. Finally, excess iRGD

and other unreacted materials were eliminated by dialysis for 3 days.

Preparation of AuNCs/DOX@Se-iRGD

AuNCs were prepared according to our previous report.[36] Na_2SeO_3 solution (100 mM) and Vc solution (100 mM) were freshly prepared. Firstly, Na_2SeO_3 solution was added dropwise to 1mL DOX solution (2 mg/mL) to a final concentration of 3 mM, and then 1.5mL AuNCs solution (300 nM) was added into the above solution drop by drop. Secondly, Vc solution was slowly added dropwise into the mixed solution to a final concentration of 12 mM. Next, 2.4 mL CS solution (0.8 mg/mL) was added into the above mixed solution. After stirring for 8 h under darkness, the AuNCs/DOX@Se solution was obtained. Finally, 500 μL of CS-iRGD was added into the AuNCs/DOX@Se solution, and then made the volume of solution to 10 mL with deionized water. Then, this solution was stirred for 12 h to complete the reaction. Unreacted materials, including the excess DOX, Na_2SeO_3 solution, Vc solution and other substances, were removed by dialysis for 3 days.

Characterization of AuNCs/DOX@Se-iRGD

The morphology of nanocomposites was observed using transmission electron microscopy (TEM Jeol JEM-2100F). X-ray diffraction (XRD, Rigaku SmartLab 9kW) was used to confirm the crystal phase. Particle sizes and zeta potentials were examined by a Zetasizer Nano-ZS from Malvern Instruments (Zetasizer Nano-SZ). The functional groups of the prepared nanocomposite were examined via a Fourier transform infrared (FTIR) spectrometer (Thermo Scientific Nicolet IS50). UV-Vis spectra were determined by using a UV-Vis spectroscopy (Agilent Cary 8454). The photothermal agents were irradiated by an 808-nm continuous-wave NIR laser (Hi-Tech Optoelectronics Co., Beijing, China). The amount of Se and Au in the nanocomposite was measured by an inductively coupled plasma-atomic emission spectrometer (ICP-OES). The amount of DOX loaded into AuNCs/DOX@Se-iRGD was determined according to a previous report.[24] Firstly, the DMSO-digesting method was used to decompose AuNCs/DOX@Se-iRGD to release the encapsulated DOX from this nanosystem. Then, the DOX concentration was measured by a multimode microplate reader (BMG LABTECH CLARIO star) with the Ex/Em wavelength at 485/590 nm to analyze drug loading capacity.

Photothermal Ability of AuNCs@Se

To evaluate the photothermal performance of the AuNCs@Se nanocomposite, AuNCs@Se in different concentrations (0, 18.75, 37.5, 75, 150, and 300 ppm) was irradiated by 808 nm laser with 1.5 W/cm^2 power for 300 seconds. To test the Se shell whether it affects the photothermal property of AuNCs, AuNCs in different concentrations (0, 3.75, 7.5,15, 30, and 60 ppm) were also irradiated under the same condition. Besides, AuNCs@Se with 150 ppm was exposed to NIR laser at various power densities (0.5, 0.75, 1.0, 1.25, and 1.5 W/cm^2) for 300 seconds. Moreover, the photothermal stability of AuNCs@Se at a concentration of 150 ppm under NIR laser (1.25 W/cm^2) was measured. The aqueous solution was irradiated until reaching its maximum temperature, and then the temperature of suspension decreased to room temperature naturally. The cycle of heating and cooling was repeated five times. All the temperatures were recorded and thermal images were captured by a thermal imager (FLUKE Ti450 IR fusion technology).

Drug Release of AuNCs/DOX@Se-iRGD in Solution Under Different Conditions

Briefly, AuNCs/DOX@SeNPs-iRGD (5mg) was dissolved in 5mL of phosphate-buffered saline (PBS) with pH of 5.3, 6.5 and 7.4 to investigate the drug release in different pH buffer solutions. The samples were irradiated with or without NIR laser (centered at 808 nm, output power = 1.0, 1.5 and 2.0 W/cm^2 for 5 mins) at the specified time points. After centrifugation for 10 min with 14,000 rpm, 300 μL of liquid supernatant was collected and then 300 μL deionized water was added into the previous solution. The amount of DOX release was measured by a multimode microplate reader.

Cell Culture and Cell Viability by MTT Assay

A cytotoxicity assay MTT was carried out in MCF-7 cells and MRC-5 cells which were purchased from the American Type Culture Collection (ATCC, Manassas, VA). The cells were cultured as described previously.[26] Cytotoxicity assay was also performed as previously reported.[26] The fluorescence images stained with calcein AM (green) and PI (red) and thermal images of MCF-7 cells with different treatments were taken by fluorescence microscopy (ZEISS Observer, Z1) and thermal imager, respectively.

Cellular Uptake

The cellular uptake of AuNCs@Se and AuNCs@Se-iRGD in MCF-7 cells and MRC-5 cells was studied by measuring the Se and Au concentrations inside the cells using inductively coupled plasma-mass spectrometry (ICP-MS) as previously described.[37] The cells were seeded in a 6-well plate and incubated for 24 h, followed by incubation with AuNCs@Se and AuNCs@Se-iRGD for 4h, gentle washing with PBS, digestion and extraction with aqua regia, and dilution with 1% HNO$_3$.

In vitro and in vivo PAI and PTT

The PA spectra and related images of these nanocomposites in vitro/in vivo were captured by the FUJIFILM Visual Sonics Vevo LAZR multi-modality imaging platform. The system included a flash lamp pumped Q-switched Nd: YAG laser with OPO that was capable of operating from 680~970 nm with a peak pulse energy of 26 mJ (at 20 Hz) and transducer LZ250 (13–24 MHz) was selected to conduct the PAI experiment. In vitro PAI:

AuNCs@Se aqueous dispersions with concentrations of 0, 0.125, 0.25, 0.5, 1.0 and 2.0 g/L were injected into individual tube phantoms and monitored by the Vevo LAZR PA Imaging System at a wavelength of 740 nm.

Female nude mice aged 4–6 weeks were purchased from the Chinese University of Hong Kong raised in the Centralised Animal Facilities of The Hong Kong Polytechnic University. After 10 days of quarantine, the body weight of each mouse was about 18–20 g, and the 100 μL of MCF-7 cells with density 1×10^7 cells/mL were suspended in serum-free DMEM and subcutaneously inoculated right hind limb of nude mice. Tumors could be formed in a week, with a tumor size of 5–6 mm. We have obtained the animal ethics approval from The Government of the Hong Kong Special Administrative Region Department of Health (Ref. (19–152) in DH/ SHS/8/2/4 Pt. 7). The procedures were performed in accordance with the Guidelines for care and use of laboratory animals of "The Special Health Service, Department of Health, Hong Kong Special Administrative Region" and approved by the Animal Ethics Committee of "The Hong Kong Polytechnic University".

As for in vivo PAI, the nude mice with a tumor size of 5–6 mm were selected and divided into two groups. AuNCs@Se and AuNCs@Se-iRGD (5 mg/mL, 0.1 mL) were injected intravenously. The mice were anesthetized with 3% isoflurane and kept at a constant temperature of 37.5°C. The PA value and images of these nanocomposites accumulated in the tumor site were sequentially collected at specific time points for 48 h.

In vivo Anti-Tumor Activity and Biosafety

As for in vivo anti-tumor activity, the mice were randomly divided into eight groups and intravenously injected with the following samples (three mice per group): G1: PBS, as a control group; G2:AuNCs@Se-iRGD; G3: DOX@Se-iRGD; G4: AuNCs/DOX@Se-iRGD; G5: PBS+Laser; G6:AuNCs@Se-iRGD+Laser; G7:DOX@Se-iRGD +Laser; and G8:AuNCs/DOX@Se-iRGD + Laser. A total of 100 μL of solution was delivered into each mouse via tail vein injection. The mice in G5, G6, G7 and G8 were anesthetized 24 hours after the injections using pentobarbital and their tumors were under irradiation (1.5 W/cm^2) for 10 mins. During the treatment, the body weight of these mice and size of the tumors were measured for 21 days. Besides, main tissues such as the tumor, heart, liver, spleen, lung and kidney were dissected, and paraffin sections were prepared and stained with hematoxylin and eosin (H&E) to observe the pathological changes caused by different treatments or manifested in the different treatment groups.

Statistical Analysis

All the experiments were repeated at least three times; results are expressed as the mean ± sd. Differences among different treatment groups were analyzed by one-way ANOVA with multiple comparisons by using SPSS13.0 statistical software.

Results and Discussion
Design and Characterization of AuNCs/ DOX@Se-iRGD

As illustrated in Scheme 1, the nanocomposite AuNCs/ DOX@Se-iRGD targeted the tumor site via the ligand–receptor interaction mechanism between iRGD on the nanocomposite and integrins that were highly overexpressed on cancer cells; effective tumor inhibition was achieved by chemo-photothermal therapy with the guidance of PAI. The synthetic procedure of AuNCs/ DOX@Se-iRGD included two main steps (Scheme 1A). The first step was the preparation of monodispersed AuNCs which were used as templates for the AuNCs@Se-iRGD core-shell nanostructure, and the second step was drug loading to AuNCs@Se-iRGD.

According to our previous work,[35] AuNCs were synthesized via template-engaged galvanic replacement reaction of Ag nanoparticles. As shown in Figure 1A and B, TEM images of AuNCs showed a uniform size of about 45 nm with a hollow structure and those of SeNPs alone showed a near-spherical morphology. After Se and CS shell formation on AuNCs, the core-shell AuNCs@Se nanocomposites showed a uniform size with near-spherical morphology (Figure 1C–E). X-ray diffraction (XRD) was used to prove the existence of Se and Au in the AuNCs@Se nanocomposites (Figure S1) which demonstrated the presence of Au (PDF: 03–065-8601) and Se (PDF: 01–073-0465). Besides, as shown in Figure S2, the existence of Se and Au in the AuNCs@Se nanocomposites was further confirmed by elemental mapping images and energy dispersive spectroscopy. Moreover, the successful assembly of Se and CS was confirmed by zeta potential measurements. AuNCs exhibited a negative surface charge (−18.4mV) due to the presence of citrate ions on the surface; Se and CS assembly switched the surface charge to a positive surface charge (+28.6 mV), indicating the presence of positively charged CS with a large amount of amines on the
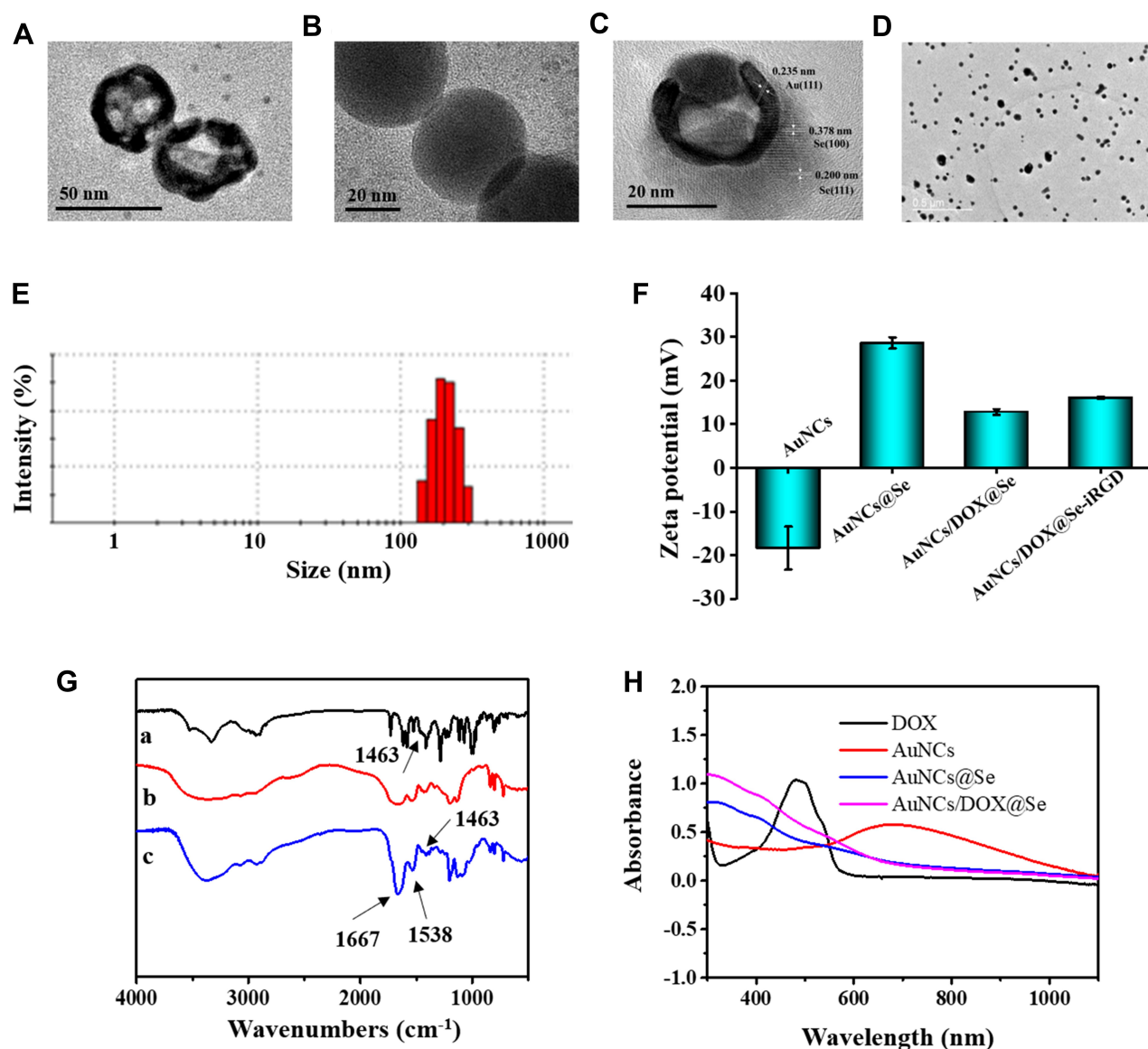
Figure 1 TEM images of (**A**) AuNCs, (**B**) SeNPs, (**C** and **D**) AuNCs@Se at different magnifications; (**E**) The size distribution of AuNCs@Se; (**F**) The zeta potential of these nanocomposites; (**G**) The FTIR spectra of (a) DOX, (b) iRGD, (c) AuNCs/DOX@Se-iRGD; (**H**) The UV-Vis spectra of DOX, AuNCs, AuNCs@Se and AuNCs/DOX@Se.

surface of the Se shell. After the loading of DOX and conjugation of iRGD, the zeta potentials of the AuNCs/DOX@Se and AuNCs/DOX@Se-iRGD nanocomposites were measured to be +12.8 mV and +16.1 mV, respectively (Figure 1F), which indicated successful drug loading and modification of iRGD when compared with AuNCs@Se-iRGD.[24] The hydrodynamic size of AuNCs/DOX@Se-iRGD was around 200 nm. The stability of AuNCs/DOX@Se-iRGD was evaluated by measuring their size when exposed to different media (PBS, and DMEM containing 10% FBS) for 3 days as shown in Figure S3. No precipitation was observed, further verifying their long-term colloidal stability in the simulated physical environment in vitro. Drug incorporation and iRGD

attachment were further confirmed by FTIR (Figure 1G). In the absorption spectrum of AuNCs/DOX@Se-iRGD, the characteristic absorbance bands at 1463 cm^{-1} could be assigned to the benzene ring modes from DOX. The stronger peaks at 1667 cm^{-1} and 1538 cm^{-1} are attributed to the C=O stretching and N-H in-plane vibration associated with amide groups. The UV-Vis spectra of AuNCs, AuNCs/Se and AuNCs/DOX@Se-iRGD were obtained using UV-Vis spectroscopy (Figure 1H). The original AuNCs showed an LSPR band at about 750 nm, whereas pure Se nanoparticles showed no absorption bands. After Se shell formation and CS modification, AuNCs@Se, similar to previously reported, showed a broadband absorption band spanning across the UV, visible

and NIR regions.[27] With the broadband absorption spectrum, AuNCs@Se is beneficial for the subsequent NIR-stimulated controlled drug release and photothermal therapy. Compared with the UV-Vis spectra of free DOX and AuNCs/Se, AuNCs/DOX@Se-iRGD exhibited the characteristic absorption of DOX at around 485 nm. Also, the loading capacity (LC) of DOX in the AuNCs/DOX@Se-iRGD was about 2.245% and the mass ratio of Se and Au in this nanosystem was 3.854:1.

Photothermal Performance and Photoacoustic Property of the AuNCs/Se Nanocomposite

The extinction coefficient (α) represents the light absorption ability of a nanocomposite, an ability that is closely related to its photothermal performance.[38] As shown in Figure 2A, AuNCs@Se NPs dispersed in aqueous solution exhibited a broad and strong band in UV-Vis spectra with an extinction coefficient (α) of 7.1 $Lg^{-1}cm^{-1}$ at 808 nm as determined by Lambert–Beer law (Figure 2B), which is higher than other proposed probes such as Ta_4C_3 MXenes (4.06 $Lg^{-1}cm^{-1}$)[39] and GO nanosheets (3.6 $Lg^{-1}cm^{-1}$).[40] This indicated AuNCs@Se NPs laid a good foundation for photothermal

application of this AuNCs/Se nanocomposite in the following study in this paper.

The photothermal behavior of AuNCs@Se NPs was evaluated by measuring temperature elevation and taking the corresponding thermal images of different concentrations of AuNCs@Se NPs solution (0, 18.75, 37.5, 75, 150, and 300 ppm) irradiated by 808 nm NIR laser at 1.5 W/cm^2 for 300 s (Figure 2C and D). The temperature of AuNCs@Se NPs increases in a concentration-dependent manner. The temperature of AuNCs@Se NPs solution could reach 75.2°C when its concentration was 300 ppm. However, pure water under the same condition did not induce any obvious temperature increase. Changes in temperature of 150 ppm of AuNCs@Se NPs suspension irradiated under a NIR laser at elevated power densities (0.5, 0.75, 1.0, 1.25, and 1.5 W/cm^2) for 300 s were also monitored (Figure 2E). The temperature of the AuNCs@Se NPs suspension increased to 61.7°C at the highest laser output power density (1.5 W/cm^2). The results demonstrated that the NIR-heating behaviors of AuNCs@Se are concentration-, power-, and time-dependent. The photothermal stability of AuNCs@Se NPs is especially crucial for the effect of photothermal
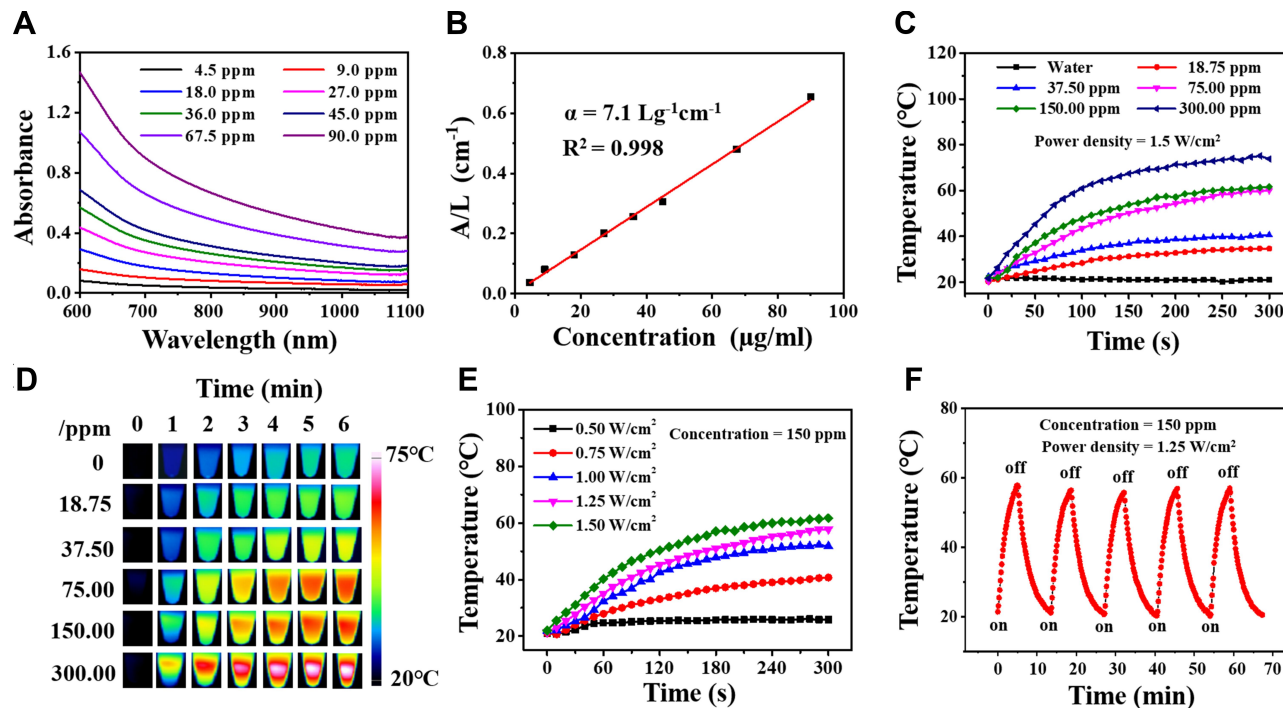

Figure 2 (**A**) The UV–Vis spectra of AuNCs@Se at different concentrations; (**B**) Normalized absorbance intensity at λ = 808 nm divided by the characteristic length of the cell (A/L) at different concentrations; (**C** and **D**) Photothermal-heating curves of AuNCs@Se and related thermal images at different concentrations (0, 18.75, 37.5, 75, 150, and 300 ppm) under 808 nm laser irradiation with the same power density of 1.5 W/cm^2 for 300 s as function of irradiation time; (**E**) Photothermal-heating curves of AuNCs@Se at concentration of 150 ppm under 808 nm laser irradiation with different power densities (0.5, 0.75, 1.0, 1.25, and 1.5 W/cm^2) as function of irradiation time; (**F**) Heating curves of AuNCs@Se for five on/off cycles under 808 nm laser irradiation.

therapy.[41,42] As shown in Figure 2F, the thermal curves of AuNCs@Se NPs remained unchanged after five heating and cooling cycles under 808 nm laser irradiation (1.25 W/cm^2), which indicated good photothermal stability of AuNCs@Se NPs after a long duration of laser irradiation. Besides, the photothermal behavior of AuNCs was investigated and compared with the same Au concentration of AuNCs@Se nanocomposites and found that these two nanocomposites exhibited similar photothermal properties. AuNCs exhibited in a concentration-dependent manner. The temperature of AuNCs with 60 ppm Au concentration could reach about 80°C (Figure S4), which is similar to that of AuNCs@Se nanocomposites (75°C, Figure 2C) under the same irradiation condition (1.5 W/cm^2 for 300 s). Hence, it indicates that the formation of Se shell on the surface of AuNCs did not obviously affect its photothermal property of the AuNCs@Se nanocomposites.

NIR-Stimulated Release of DOX

The release of DOX from AuNCs/DOX@Se-iRGD could be readily controlled with NIR laser irradiation and manipulation of pH as in Figure 3A. It was observed that a small amount of DOX was released in pH 7.4 buffer. However, incremental release of encapsulated DOX (about 64% and 52% of total loading) was observed over 36 h at lower pH 5.3 and pH 6.5, respectively (Figure S5 and Figure 3B). This was attributed to the Se deformation of nanocomposite in acidic solution but not in neutral condition. The amount of drug released from AuNCs/DOX@Se-iRGD after 2 h and 8 h of NIR irradiation showed a dramatic increase compared with that without laser irradiation. Additionally, an elevated laser power density could trigger more drug release. For instance, the cumulative drug release of all encapsulated DOX under 2.0 W/cm^2 irradiation in pH 6.5 solution could reach 70.3%, which was more than that under 1.5 and 1.0 W/cm^2 (63.8% and 58.7%, respectively). Enhanced DOX release triggered by NIR laser was attributed to the heat generated from AuNCs as a result of hyperthermia-induced collapse.

The morphology of the nanocomposite after drug release was investigated using TEM. The structure of AuNCs/DOX@Se-iRGD collapsed due to the deformation of the exterior Se shell when incubated in acidic condition (Figure 3C). Moreover, except for the Se shells, the core AuNCs of the nanocomposite were also out of shape after hyperthermia treatment (Figure 3D). These results indicated that the nanocomposite could dissociate in acidic condition

and hyperthermia and thus trigger drug release in a controlled manner.

In vitro Cellular Uptake Assay

Effective targeting can improve the anti-tumor activity of the nanocomposite and reduce the damages of chemotherapy drugs to normal tissues because the effectiveness of targeting is an important criterion to evaluate the availability of nanocarriers.[27] The $\alpha_v\beta_3$ integrin is overexpressed in cancer cells such as MCF-7 cells but not in normal cells such as MRC-5 cells, and iRGD peptide could penetrate into tumor tissue and target tumor cells by binding to $\alpha_v\beta_3$ integrin. Therefore, these two different cell lines were selected to evaluate the targeting effect of this probe. To investigate the affinity of AuNCs@Se-iRGD to cancer cells, ICP-MS was performed to analyze Se and Au uptake by cancer cells (MCF-7) and normal cells (MRC-5) (Figure S6). The uptake amounts of these nanocomposites determined by Se concentration was consistent with those determined by Au concentration. Obviously, both MCF-7 and MRC-5 cells exhibited gradually enhanced uptake of AuNCs@Se-iRGD with the increase of incubation time. At the same incubation time point, the uptake of AuNCs@Se-iRGD in MCF-7 cells was obviously higher than that in MRC-5 cells, whereas there were no obvious uptake differences in the uptake of the non-targeting AuNCs@Se nanocomposite between MCF-7 cells and MRC-5 cells. To verify the role of the iRGD-mediated pathway, MCF-7 cells were first incubated with free iRGD peptide for 4 h to block the integrin receptor on the cancer cell membranes, and then the cells were incubated with AuNCs@Se-iRGD for another 4 h. As shown in Figure S7, the internalization of AuNCs@Se-iRGD was distinctly inhibited by the iRGD peptide in a concentration-dependent manner, which indicated that the efficient and selective cellular uptake of AuNCs@Se-iRGD in MCF-7 cells was enhanced by the iRGD-mediated mechanism.[43,44]

In vitro Chemo-Photothermal Synergistic Therapy Against MCF-7 Cells

The cytotoxicity of AuNCs/DOX@Se-iRGD, AuNCs@Se-iRGD and DOX@Se-iRGD was examined against MCF-7 cells by MTT assay. As shown in Figure 3E, the IC$_{50}$ values of AuNCs/DOX@Se-iRGD (18.3 μM) and DOX@Se-iRGD (18.0 μM) showed no significant differences, but are much lower than that of AuNCs@Se-iRGD (120.7
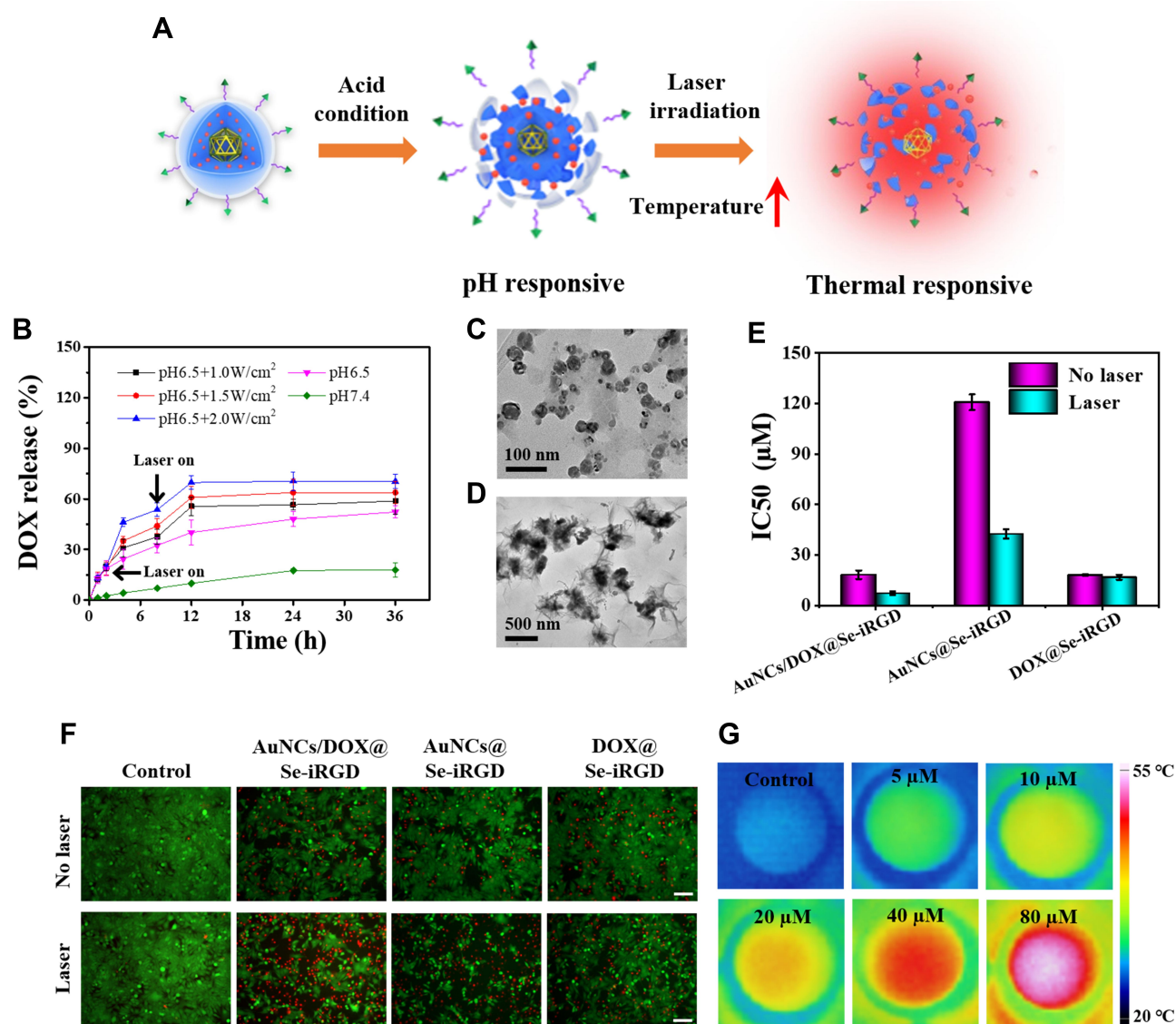
Figure 3 (**A**) Schematic illustration of pH plus photothermal triggered drug release from AuNCs/DOX@Se-iRGD; (**B**) DOX release curves from AuNCs/DOX@Se-iRGD in PBS buffer at pH 7.4 and pH 6.5, with and without the NIR laser irradiation; (**C** and **D**) TEM images of AuNCs/DOX@Se-iRGD in acid condition without and with NIR lasers irradiation; (**E**) The IC$_{50}$ values of MCF-7 cells with different treatments; (**F**) Fluorescent images of calcein AM (green) and PI (red) stained MCF-7 cells treated with PBS, AuNCs/DOX@Se-iRGD, AuNCs@Se-iRGD and DOX@Se-iRGD (with without laser, the concentrations of Se was 10 μM), all scale bars are 50 μm; (**G**) The thermal images of MCF-7 cells treated with AuNCs/DOX@Se-iRGD and NIR laser irradiation. Data are shown as the mean ± standard deviation (SD).

μM) without NIR laser irradiation. These results indicated that pure nanocarrier AuNCs@Se-iRGD had a slight influence on cell viability. Besides, the chemo-photothermal synergistic anti-cancer ability of the nanocomposites was investigated. For example, the IC$_{50}$ of AuNCs@Se-iRGD with NIR irradiation was 42.5 μM, which is much lower than that without NIR irradiation; the IC$_{50}$ of AuNCs/DOX@Se-iRGD with NIR irradiation was determined to be 7.31 μM, but the killing efficacy of DOX@Se-iRGD showed no obvious differences with or without NIR irradiation. To further verify the synergistic effect of AuNCs/DOX@Se-iRGD in vitro, MCF-7 cells were incubated

with the nanocomposites (AuNCs/DOX@Se-iRGD, AuNCs@Se-iRGD and DOX@Se-iRGD, respectively) for 6 h, then exposed to NIR laser at 2 W/cm^2 for 5 min, followed by a further incubation for 18 h; a control was done without laser irradiation. The cells were stained with calcein AM and propidium iodide (PI) to evaluate the cell viability. Calcein AM would enter live cells and emit green fluorescence, while PI would only penetrate the dead cells and emit red fluorescence. It was clear from these fluorescence images that the majority of cells incubated with AuNCs/DOX@Se-iRGD with laser irradiation showed much more red fluorescence than cells that received other

treatments, indicating more cells were dead (Figure 3F). Besides, the photothermal images of MCF-7 cells incubated with elevated concentrations of AuNCs/DOX@Se-iRGD (Figure 3G) indicated that the nanocomposite could enhance temperature in a concentration-dependent manner in cells. Isobologram analysis was employed to determine the inhibitory effect of the chemo- and photothermal synergistic therapy. As shown in Figure S8, the data point in the isobologram was far below the line defining the additive effect, indicating the nanocomposite could achieve chemo-photothermal synergistic therapy with NIR irradiation. These results demonstrated that our AuNCs/DOX@Se-iRGD nanocomposite could successfully achieve the synergistic effect of chemo- and photothermal therapy for killing cancer cells, which is attributed to the effective conversion of NIR light into heat by the AuNCs, resulting in the hyperthermia- and pH-induced collapse of the Se shell that triggered DOX release from the nanocarrier.

In vivo PAI and Photothermal Imaging

To explore the feasibility of employing AuNCs@Se for PAI of MCF-7 cells in vivo, PA phantom studies were performed (Figure 4A and B). A quantitative PA signal intensity change versus concentration of AuNCs@Se was observed ($R^2 = 0.9918$). Next, the in vivo PA images and the corresponding signals of tumor site were investigated at different time intervals (0, 4, 8, 12, 24, and 48 h) after intravenous injection of the AuNCs@Se-iRGD and AuNCs@Se nanocomposites. As shown in Figure 4C and D, an intense PAI signal in tumor site could be easily observed after intravenous injection of the nanocomposites into the tumor-bearing mice. The PAI signal of AuNCs@Se in the tumor site gradually increased and reached its highest value at 12 h (1.31 a.u.), and then steadily declined to 0.32 a.u. within 48 h. However, for AuNCs@Se-iRGD, the average signal showed an obvious upward trend from 0.18 a.u. to 3.59 a.u., indicating a time-dependent accumulation at the tumor; after peaking at 24 h, the signal went back to 1.81 a.u. at 48 h, which suggested clearance of the nanocomposites from the tumor site. Therefore, the 24 h post-injection time was selected as the time point of photothermal therapy. The PA signal intensity of AuNCs@Se-iRGD was consistently higher than that of AuNCs@Se and the enhanced tumor PA signal was attributed to the modification of the target peptide onto the nanocomposite surfaces.

A photothermal imaging study of AuNCs@Se-iRGD was also carried out using MCF-7 tumor-bearing mice model. At 24 h after treatment via the tail vein, tumors were exposed to laser irradiation at different power (0, 0.5, 1.0, 1.5 W/cm²) for 10 mins (Figure 4E and F). During this irradiation, the temperature of the tumor tissue increased dramatically and exhibited a laser power density-dependency. As shown in Figure 4E, when irradiated with 1.5 W/cm² laser, the temperature of the tumor site quickly increased to 45.9°C, which was enough to ablate tumor tissue because this temperature could be regarded as mild hyperthermia therapy when combined with other treatments at 39–42°C.[45] The surrounding healthy tissue showed negligible temperature increase. No obvious temperature changes were observed in the control group with PBS treatment.

In vivo Chemo-Photothermal Synergistic Therapy

The anti-tumor activity of AuNCs/DOX@Se-iRGD was determined by the MCF-7 cancer cell xenografted mice model. Compared with the groups treated with AuNCs@Se-iRGD + Laser (group 6), the tumor volumes of the AuNCs@Se-iRGD group (group 2) had a smaller enlargement (Figure 5A). This indicated that the nanosystem-induced photothermal therapy had a little inhibitory effect on the tumor. The therapeutic efficacy observed from the AuNCs/DOX@Se-iRGD + Laser group (group 8) was much higher than other groups. The enhanced anti-tumor efficacy of group 8 was mainly a result of the synergistic interaction of chemo-photothermal therapy. All the mice were sacrificed and their corresponding tumors were extracted. As displayed in Figure 5B–D, the tumor size and weight in the mice in group 8 were significantly inhibited, whereas those in groups 6, 4, 3 and 7 displayed little or negligible inhibition. The body weights of the animals did not show an obvious fluctuation during the treatment period (Figure 5E). The main organs of the mice were collected and subjected to H&E staining. As shown in Figure 5F, no obvious organ damages or inflammatory lesions in different tissue were observed compared with the control groups. These results demonstrated that the nanocomposite had relatively low toxicity in vivo and had few side effects, making AuNCs/DOX@Se-iRGD a safe nanomedicine for cancer theranostics.

Conclusion

AuNCs/DOX@Se-iRGD nanocomposite was successfully designed and synthesized as a novel therapeutic agent for
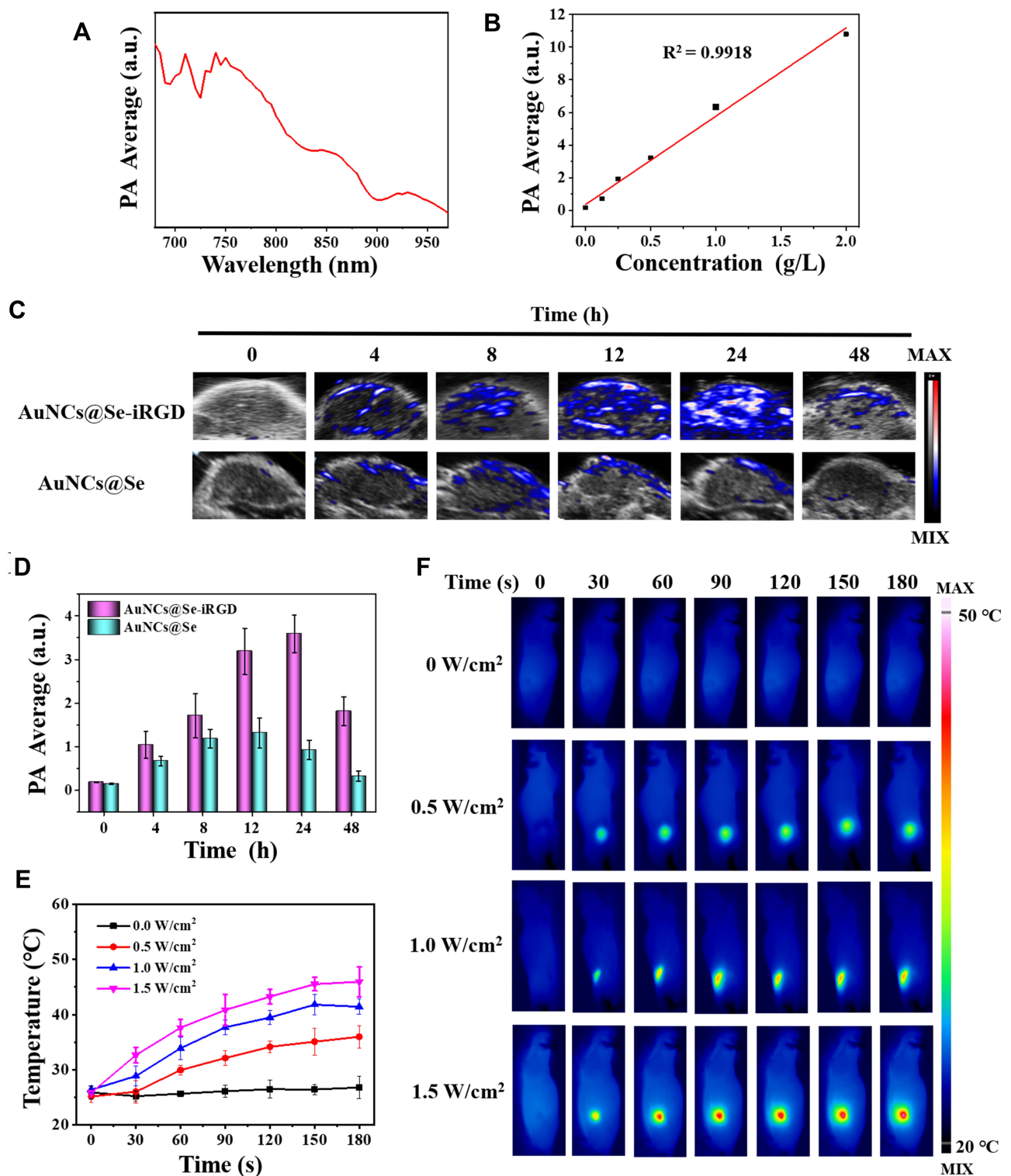
Figure 4 (**A**) PA imaging spectrum of AuNCs@Se from 680 nm to 970 nm; (**B**) PA signals of AuNCs@Se at elevated concentration in vitro; (**C** and **D**) PA images and signals of tumor site at different time intervals (0, 4, 8, 12, 24, 48 h) after i.v. injection of AuNCs@Se-iRGD and AuNCs@Se in vivo; (**E** and **F**) Thermal curves and related images of temperature changes of MCF-7 tumor-bearing mice after 24 h i.v. injection of AuNCs@Se-iRGD under various power densities.

high-efficient PAI-guided cancer chemo-photothermal synergistic therapy. The high photothermal conversion ability of AuNCs and the effective release of DOX indicated successful hyperthermia-responsive drug release behavior of this nanocomposite. The CS-iRGD surface decoration significantly enhanced the cellular uptake of the nanocomposite in cancer
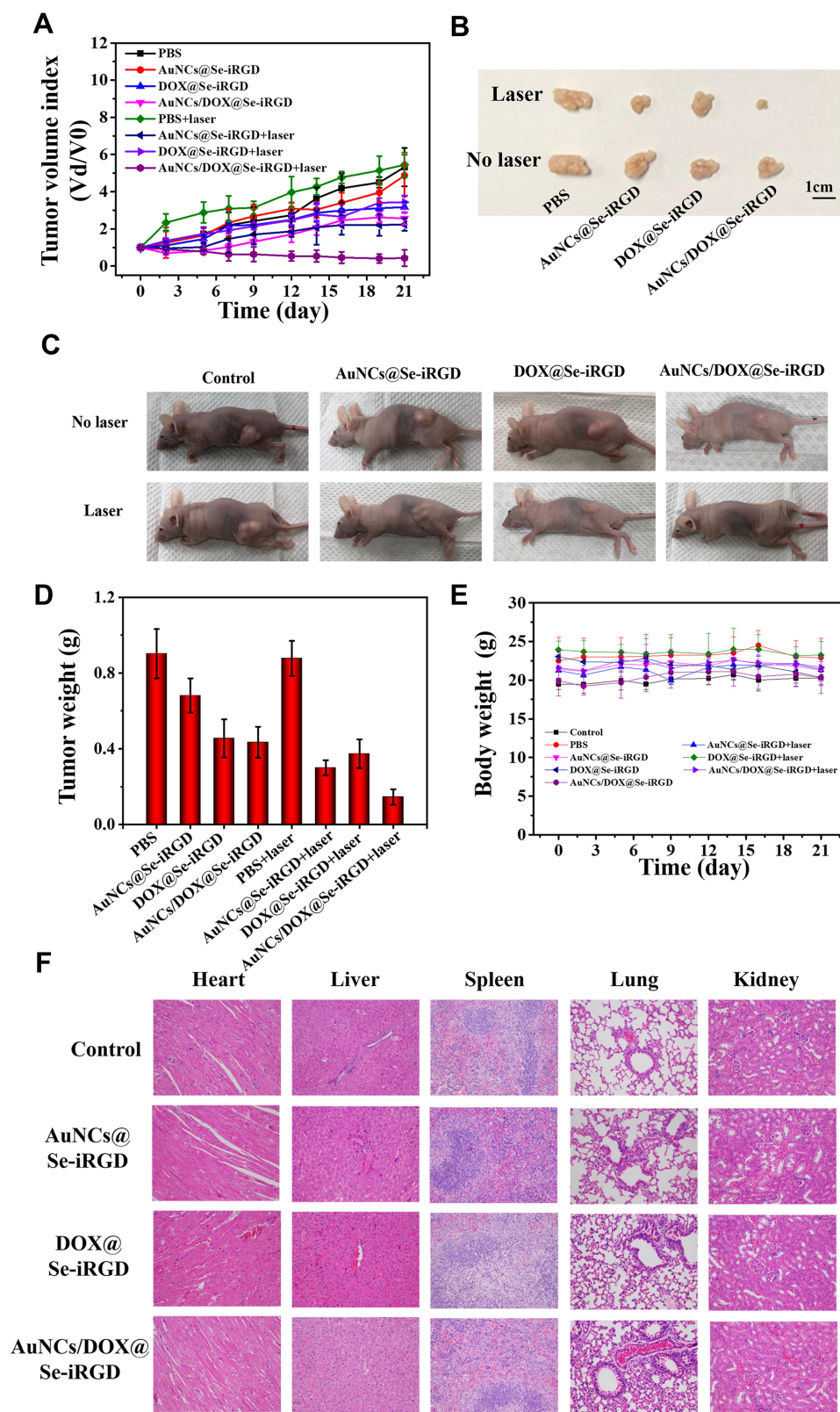
Figure 5 (**A**) Tumor volume index of tumor-bearing mice for different treatments during the 21 days observation period; (**B**) Representative pictures of tumors collected from different groups in the 21st day; (**C**) Representative pictures of typical mice after different treatments in the 21st day; (**D**) Tumor weight of tumor-bearing mice collected from different groups in the 21st day; (**E**) The body weight curves of tumor-bearing mice during the 21 days observation period; (**F**) Histology analysis of the major organs from different treatment group in the 21st day.

cells, leading to increased tumor targeting capacity. The enhanced antitumor growth effect suggested that the combination of chemo-, photothermal and Se-based therapy showed great potential in breast cancer treatment. Meanwhile, PAI presented its superiority in imaging-guided monitoring and therapy. These findings provide a new opportunity for achieving desired therapeutic effects using AuNCs-based nanoplatform for breast cancer therapy.

Acknowledgments

Disclosure

The authors report no conflicts of interest in this work.

References

1. Siegel RL, Miller KD, Jemal A. Cancer statistics, 2017. *CA Cancer J Clin*. 2017;67(1):7–30. doi:10.3322/caac.21387
2. Emens LA. Breast cancer immunotherapy: facts and hopes. *Clin Cancer Res*. 2018;24(3):511–520. doi:10.1158/1078-0432.CCR-16-3001
3. Jabr-Milane LS, van Vlerken LE, Yadav S, Amiji MM. Multifunctional nanocarriers to overcome tumor drug resistance. *Cancer Treat Rev*. 2008;34(7):592–602. doi:10.1016/j.ctrv.2008.04.003
4. Wang LM, Sun Q, Wang X, et al. Using hollow carbon nanospheres as a light-induced free radical generator to overcome chemotherapy resistance. *J Am Chem Soc*. 2015;137(5):1947–1955. doi:10.1021/ja511560b
5. Li Z, Hu Y, Miao Z, et al. Dual-stimuli responsive bismuth nanoraspberries for multimodal imaging and combined cancer therapy. *Nano Lett*. 2018;18(11):6778–6788. doi:10.1021/acs.nanolett.8b02639
6. Liang C, Xu L, Song G, Liu Z. Emerging nanomedicine approaches fighting tumor metastasis: animal models, metastasis-targeted drug delivery, phototherapy, and immunotherapy. *Chem Soc Rev*. 2016;45(22):6250–6269. doi:10.1039/c6cs00458j
7. Chen Q, Liang C, Wang C, Liu Z. An imagable and photothermal "abraxane-like" nanodrug for combination cancer therapy to treat subcutaneous and metastatic breast tumors. *Adv Mater*. 2015;27(5):903–910. doi:10.1002/adma.201404308
8. Davoodi P, Lee LY, Xu Q, et al. Drug delivery systems for programmed and on-demand release. *Adv Drug Deliv Rev*. 2018;132:104–138. doi:10.1016/j.addr.2018.07.002
9. Zhao X, Yang C-X, Chen L-G, Yan X-P. Dual-stimuli responsive and reversibly activatable theranostic nanoprobe for precision tumor-targeting and fluorescence-guided photothermal therapy. *Nat Commun*. 2017;8. doi:10.1038/ncomms14998
10. Mai BT, Fernandes S, Balakrishnan PB, Pellegrino T. Nanosystems based on magnetic nanoparticles and thermo- or pH-responsive polymers: an update and future perspectives. *Accounts Chem Res*. 2018;51(5):999–1013. doi:10.1021/acs.accounts.7b00549

11. Cheng R, Meng FH, Deng C, Klok HA, Zhong ZY. Dual and multi-stimuli responsive polymeric nanoparticles for programmed site-specific drug delivery. *Biomaterials*. 2013;34(14):3647–3657. doi:10.1016/j.biomaterials.2013.01.084
12. Sun TM, Wang YC, Wang F, et al. Cancer stem cell therapy using doxorubicin conjugated to gold nanoparticles via hydrazone bonds. *Biomaterials*. 2014;35(2):836–845. doi:10.1016/j.biomaterials.2013.10.011
13. Qiu M, Wang D, Liang WY, et al. Novel concept of the smart NIR-light-controlled drug release of black phosphorus nanostructure for cancer therapy. *Proc Natl Acad Sci USA*. 2018;115(3):501–506. doi:10.1073/pnas.1714421115
14. Wang C, Xu H, Liang C, et al. Iron oxide@polypyrrole nanoparticles as a multifunctional drug carrier for remotely controlled cancer therapy with synergistic antitumor effect. *ACS Nano*. 2013;7(8):6782–6795. doi:10.1021/nn4017179
15. Liao JF, Li WT, Peng JR, et al. Combined cancer photothermal-chemotherapy based on doxorubicin/gold nanorod-loaded polymersomes. *Theranostics*. 2015;5(4):345–356. doi:10.7150/thno.10731
16. Liu HY, Chen D, Li LL, et al. Multifunctional gold nanoshells on silica nanorattles: a platform for the combination of photothermal therapy and chemotherapy with low systemic toxicity. *Angew Chem Int Ed*. 2011;50(4):891–895. doi:10.1002/anie.201002820
17. Ma M, Chen HR, Chen Y, et al. Au capped magnetic core/mesoporous silica shell nanoparticles for combined photothermo-/chemotherapy and multimodal imaging. *Biomaterials*. 2012;33(3):989–998. doi:10.1016/j.biomaterials.2011.10.017
18. Sun HP, Su JH, Meng QS, et al. Cancer cell membrane-coated gold nanocages with hyperthermia-triggered drug release and homotypic target inhibit growth and metastasis of breast cancer. *Adv Funct Mater*. 2017;27(3):1604300. doi:10.1002/adfm.201604300
19. Xu QB, Wan JS, Bie NN, et al. A biomimetic gold nanocages-based nanoplatform for efficient tumor ablation and reduced inflammation. *Theranostics*. 2018;8(19):5362–5378. doi:10.7150/thno.27631
20. Yavuz MS, Cheng YY, Chen JY, et al. Gold nanocages covered by smart polymers for controlled release with near-infrared light. *Nat Mater*. 2009;8(12):935–939. doi:10.1038/Nmat2564
21. Shi P, Qu KG, Wang JS, Li M, Ren JS, Qu XG. pH-responsive NIR enhanced drug release from gold nanocages possesses high potency against cancer cells. *Chem Commun*. 2012;48(61):7640–7642. doi:10.1039/c2cc33543c
22. Yang JP, Shen DK, Zhou L, et al. Spatially confined fabrication of core-shell gold nanocages@mesoporous silica for near-infrared controlled photothermal drug release. *Chem Mater*. 2013;25(15):3030–3037. doi:10.1021/cm401115b
23. Rayman MP. The importance of selenium to human health. *Lancet*. 2000;356(9225):233–241. doi:10.1016/S0140-6736(00)02490-9
24. Huang YY, He LZ, Liu W, et al. Selective cellular uptake and induction of apoptosis of cancer-targeted selenium nanoparticles. *Biomaterials*. 2013;34(29):7106–7116. doi:10.1016/j.biomaterials.2013.04.067
25. Liu T, Lai LH, Song ZH, Chen TF. A sequentially triggered nanosystem for precise drug delivery and simultaneous inhibition of cancer growth, migration, and invasion. *Adv Funct Mater*. 2016;26(43):7775–7790. doi:10.1002/adfm.201604206
26. Fang XY, Wu XL, Li CE, et al. Targeting selenium nanoparticles combined with baicalin to treat HBV-infected liver cancer. *RSC Adv*. 2017;7(14):8178–8185. doi:10.1039/c6ra28229f
27. Chang YZ, He LZ, Li ZB, et al. Designing core-shell gold and selenium nanocomposites for cancer radiochemotheray. *ACS Nano*. 2017;11(5):4848–4858. doi:10.1021/acsnano.7b01346
28. Ramasamy T, Ruttala HB, Sundaramoorthy P, et al. Multimodal selenium nanoshell-capped Au@mSiO2 nanoplatform for NIR-responsive chemo-photothermal therapy against metastatic breast cancer. *NPG Asia Mater*. 2018;10:197–216. doi:10.1038/s41427-018-0034-5

29. Dinish US, Song ZG, Ho CJH, et al. Single molecule with dual function on nanogold: biofunctionalized construct for in vivo photo-acoustic imaging and sers biosensing. *Adv Funct Mater*. 2015;25 (15):2316–2325. doi:10.1002/adfm.201404341

30. Nie LM, Wang SJ, Wang XY, et al. In vivo volumetric photoacoustic molecular angiography and therapeutic monitoring with targeted plasmonic nanostars. *Small*. 2014;10(8):1585–1593. doi:10.1002/smll.201302924

31. Li WY, Brown PK, Wang LHV, Xia YN. Gold nanocages as contrast agents for photoacoustic imaging. *Contrast Media Mol I*. 2011;6 (5):370–377. doi:10.1002/cmmi.439

32. Weber J, Beard PC, Bohndiek SE. Contrast agents for molecular photoacoustic imaging. *Nat Methods*. 2016;13(8):639–650. doi:10.1038/Nmeth.3929

33. Chen Q, Liang C, Sun XQ, et al. H_2O_2-responsive liposomal nanoprobe for photoacoustic inflammation imaging and tumor theranostics via in vivo chromogenic assay. *Proc Natl Acad Sci USA*. 2017;114 (21):5343–5348. doi:10.1073/pnas.1701976114

34. Reinhardt CJ, Chan J. Development of photoacoustic probes for in vivo molecular imaging. *Biochemistry-Us*. 2018;57(2):194–199. doi:10.1021/acs.biochem.7b00888

35. Song ZH, Chang YZ, Xie HH, Yu XF, Chu PK, Chen TF. Decorated ultrathin bismuth selenide nanosheets as targeted theranostic agents for in vivo imaging guided cancer radiation therapy. *NPG Asia Mater*. 2017;9:e439–e439. doi:10.1038/am.2017.167

36. Liu C, Li SY, Gu YJ, Xiong HH, Wong WT, Sun L. Multispectral photoacoustic imaging of tumor protease activity with a gold nanocage-based activatable probe. *Mol Imaging Biol*. 2018;20 (6):919–929. doi:10.1007/s11307-018-1203-1

37. Fang XY, Jiang WT, Huang YY, Yang F, Chen TF. Size changeable nanosystems for precise drug controlled release and efficient overcoming of cancer multidrug resistance. *J Mater Chem B*. 2017;5 (5):944–952. doi:10.1039/c6tb02361d

38. Li ZL, Zhang H, Han J, Chen Y, Lin H, Yang T. Surface nanopore engineering of 2D mxenes for targeted and synergistic multitherapies of hepatocellular carcinoma. *Adv Mater*. 2018;30(25). doi:10.1002/adma.201706981

39. Lin H, Wang Y, Gao S, Chen Y, Shi J. Theranostic 2D Tantalum Carbide (MXene). *Adv Mater*. 2018;30(4):1703284. doi:10.1002/adma.201703284

40. Robinson J, Tabakman S, Liang Y, et al. Ultrasmall reduced graphene oxide with high near-infrared absorbance for photothermal therapy. *J Am Chem Soc*. 2011;133(17):6825–6831. doi:10.1021/ja2010175

41. Huang YY, Mei CM, Tian YQ, Nie TQ, Liu Z, Chen TF. Bioinspired tumor-homing nanosystem for precise cancer therapy via reprogramming of tumor-associated macrophages. *NPG Asia Mater*. 2018;10:1002–1015. doi:10.1038/s41427-018-0091-9

42. Ma XW, Wang YY, Liu XL, et al. Fe_3O_4-Pd janus nanoparticles with amplified dual-mode hyperthermia and enhanced ROS generation for breast cancer treatment. *Nanoscale Horiz*. 2019;4(6):1450–1459. doi:10.1039/c9nh00233b

43. Cun XL, Chen JT, Ruan SB, et al. A novel strategy through combining iRGD peptide with tumor-microenvironment-responsive and multistage nanoparticles for deep tumor penetration. *ACS Appl Mater Inter*. 2015;7(49):27458–27466. doi:10.1021/acsami.5b09391

44. Puig-Saus C, Rojas LA, Laborda E, et al. iRGD tumor-penetrating peptide-modified oncolytic adenovirus shows enhanced tumor transduction, intratumoral dissemination and antitumor efficacy. *Gene Ther*. 2014;21(8):767–774. doi:10.1038/gt.2014.52

45. Mei CM, Wang N, Zhu XQ, Wong KH, Chen TF. Photothermal-controlled nanotubes with surface charge flipping ability for precise synergistic therapy of triple-negative breast cancer. *Adv Funct Mater*. 2018;28(45). doi:10.1002/adfm.201805225